

# Coupled liquid crystalline oscillators in Huygens' synchrony

**Citation for published version (APA):**

Vantomme, G., Elands, L. C. M., Gelebart, A. H., Meijer, E. W., Pogromsky, A. Y., Nijmeijer, H., & Broer, D. J. (2021). Coupled liquid crystalline oscillators in Huygens' synchrony. *Nature Materials*, 20(12), 1702-1706. Advance online publication. <https://doi.org/10.1038/s41563-021-00931-6>

**Document license:**

TAVERNE

**DOI:**

[10.1038/s41563-021-00931-6](https://doi.org/10.1038/s41563-021-00931-6)

**Document status and date:**

Published: 01/12/2021

**Document Version:**

Publisher's PDF, also known as Version of Record (includes final page, issue and volume numbers)

**Please check the document version of this publication:**

- A submitted manuscript is the version of the article upon submission and before peer-review. There can be important differences between the submitted version and the official published version of record. People interested in the research are advised to contact the author for the final version of the publication, or visit the DOI to the publisher's website.
- The final author version and the galley proof are versions of the publication after peer review.
- The final published version features the final layout of the paper including the volume, issue and page numbers.

[Link to publication](#)

**General rights**

Copyright and moral rights for the publications made accessible in the public portal are retained by the authors and/or other copyright owners and it is a condition of accessing publications that users recognise and abide by the legal requirements associated with these rights.

- Users may download and print one copy of any publication from the public portal for the purpose of private study or research.
- You may not further distribute the material or use it for any profit-making activity or commercial gain
- You may freely distribute the URL identifying the publication in the public portal.

If the publication is distributed under the terms of Article 25fa of the Dutch Copyright Act, indicated by the "Taverne" license above, please follow below link for the End User Agreement:

[www.tue.nl/taverne](http://www.tue.nl/taverne)

**Take down policy**





If you believe that this document breaches copyright please contact us at:

[openaccess@tue.nl](mailto:openaccess@tue.nl)

providing details and we will investigate your claim.



# Coupled liquid crystalline oscillators in Huygens' synchrony

Ghislaine Vantomme<sup>1,2</sup>  , Lars C. M. Elands<sup>3</sup>, Anne Helene Gelebart<sup>1,4</sup>, E. W. Meijer<sup>1,2</sup>, Alexander Y. Pogromsky<sup>3,5</sup>, Henk Nijmeijer<sup>1,3</sup> and Dirk J. Broer<sup>1,4</sup>  

**In the flourishing field of soft robotics, strategies to embody communication and collective motion are scarce. Here we report the synchronized oscillations of thin plastic actuators by an approach reminiscent of the synchronized motion of pendula and metronomes. Two liquid crystalline network oscillators fuelled by light influence the movement of one another and display synchronized oscillations in-phase and anti-phase in a steady state. By observing entrainment between the asymmetric oscillators we demonstrate the existence of coupling between the two actuators. We qualitatively explain the origin of the synchronized motion using a theoretical model and numerical simulations, which suggest that the motion can be tuned by the mechanical properties of the coupling joint. We thus anticipate that the complex synchronization phenomena usually observed in rigid systems can also exist in soft polymeric materials. This enables the use of new stimuli, featuring an example of collective motion by photo-actuation.**

Polymers able to sense, adapt, communicate and move constitute a promising class of materials for soft robotics<sup>1,2</sup>. Although many examples of actuators performing a plethora of movements have been reported<sup>3–7</sup>, the actuators are independent of one another in their motion. Yet, synchronization and collective motion are ubiquitous in nature, from the circadian rhythm to the cardiac pacemaker cells<sup>8–11</sup>. The first report of synchronization of periodic systems dates from 1665, when the Dutch scientist Huygens, inventor of the pendulum clock, observed that two identical clocks synchronized their oscillations with the two pendula swinging in opposite directions<sup>12,13</sup>. Recent work has confirmed that the coupling between the two pendula is caused by tiny mechanical vibrations travelling in the wooden structure on which the clocks are mounted<sup>14</sup>. Similar experiments have been achieved with a large number of metronomes swinging together in synchrony when placed on a freely moving base<sup>15</sup>.

To achieve collective motion, conventional robots are operated by rigid components (sensors, circuits, data processors, power sources and so on) integrated into the rigid structure of the robots<sup>16,17</sup>. In soft robotics, instead, devices are constructed with compliant soft materials and the communication functions should be implemented into the material without the use of external rigid devices. Current strategies to embody communication mechanisms with soft components rely on chemical signalling<sup>18–20</sup>, optical properties<sup>21,22</sup> and sensing with electronic skins<sup>23,24</sup>. The next step of translating these communication mechanisms into synchronized movements needs to be achieved for realizing collective motion in soft robotics.

Although many external stimuli are reported for coupled oscillators, the use of light is a logical but missing stimulus to arrive at mechanical oscillation, most probably due to the rigidity of the pendula used so far. The lack of examples using light<sup>25</sup> to obtain coupled oscillations is the more unexpected as nature often uses light to

synchronize and create collective motion. Inspired by the work on synchrony and spurred on to develop strategies for coordinated motion in soft materials, we study the motion of coupled plastic oscillators fuelled by light.

## Collective synchronization

Inspired by the work on synchrony of Huygens, we report here on the collective synchronized motion of thin plastic films upon light irradiation. Thereto, two oscillating actuators interact and influence the movement of one another by coupling their oscillation in-phase and anti-phase in a steady state. The synchronization is controlled by a coupling element, which is a piece of film joining the two oscillators. To explain qualitatively the origin of the synchronized motion, a model was put forward using mechanical coupling in the joint of the oscillators. In-phase and anti-phase motion were modelled by tuning the stiffness and the damping of the coupling joint. These results demonstrate a communication mechanism and synchronized motion in soft actuators and provide new approaches for the development of complex motion.

These actuators are thin films of liquid crystal networks<sup>26</sup> (LCNs) and they oscillate continuously under light irradiation due to a self-shadowing effect<sup>27,28</sup>. The mechanism of oscillation differs from the first report of photo-induced LCNs oscillation, which is based on the reorientation of photoswitches in the polymer network<sup>29</sup>. Here, the LCN film consists of photocrosslinked mesogenic monomers with a gradient in their molecular alignment. On average the molecules are oriented perpendicular to the film surface at one side of the film and parallel to the long axis of the film at the opposite side. The bending of the LCN is induced by light absorption of an added chromophore by exposure with a collimated light emitting diode, which heats the film locally (Extended Data Fig. 1). This changes the scalar order parameter and results in thermally induced

<sup>1</sup>Institute for Complex Molecular Systems, Eindhoven University of Technology, Eindhoven, the Netherlands. <sup>2</sup>Department of Chemical Engineering and Chemistry, Laboratory of Macromolecular and Organic Chemistry, Eindhoven University of Technology, Eindhoven, the Netherlands. <sup>3</sup>Department of Mechanical Engineering, Dynamics and Control, Eindhoven University of Technology, Eindhoven, the Netherlands. <sup>4</sup>Department of Chemical Engineering and Chemistry, Laboratory for Functional Organic Materials and Devices, Eindhoven University of Technology, Eindhoven, the Netherlands. <sup>5</sup>Department of Control Systems and Industrial Robotics, Saint-Petersburg National Research University of Information Technologies Mechanics and Optics, Petersburg, Russia. ✉e-mail: [g.vantomme@tue.nl](mailto:g.vantomme@tue.nl); [d.broer@tue.nl](mailto:d.broer@tue.nl)

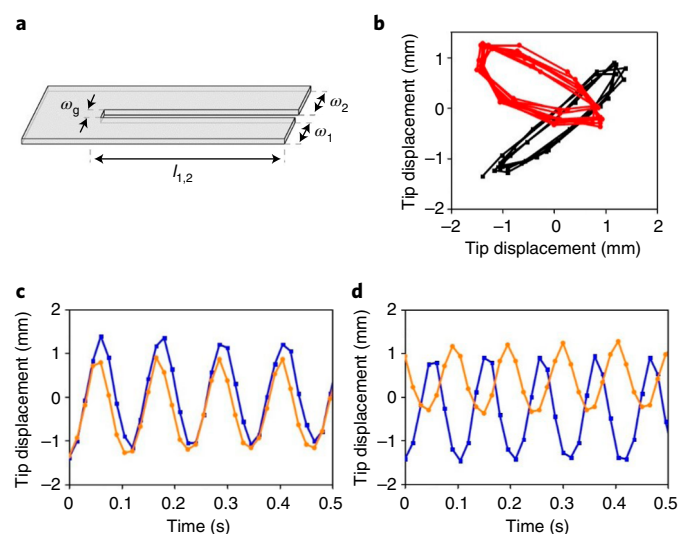


**Fig. 1 | Synchronized light-induced oscillation of coupled LCN films.**

**a**, Schematic representation of the oscillators with their dimensions. The film geometry is 15 mm ( $l_{1,2}$ , length of the films)  $\times$  4 mm ( $w_1 = w_2$ , width of the films). They are connectively separated by 2 mm ( $w_g$ ). The sample thickness is 20  $\mu\text{m}$ . **b**, Phase diagrams of the in-phase (black trace) and anti-phase (red trace) oscillators. **c,d**, Displacement of the oscillators tips over time in the z-direction showing in-phase oscillation (**c**) and anti-phase oscillation (**d**). The displacement of one oscillator is represented with the orange trace and the other one with the blue trace.

expansion at the side with perpendicular orientation and contraction at the side with planar orientation, and therefore bending occurs at the location of the heated spot (hinge). When the film bends up, its end shadows the hinge, which cools down, forcing the film to bend back in the direction of its original position. This process repeats and brings the film into light-driven oscillation in accordance with its natural frequency as determined by its size and mechanical properties. The frequency can be tuned by changing the stiffness and/or the dimensions, which have been carefully optimized for the purpose of the experiments presented here<sup>27,28,30</sup>. The frequency goes up with increasing modulus and decreasing length of the film.

When a rectangular piece of a LCN film is split down the middle, creating two strip-like oscillators connected by a joint of the same material (Fig. 1a), the two oscillators show synchronized motion upon light irradiation (LED 365 nm, 0.5 W/cm<sup>2</sup>). The oscillators move with the same period and amplitude at the same time, and their motion is coupled in-phase (Fig. 1c and Supplementary Video 1). The frequency of the oscillation is 8.5 Hz  $\pm$  0.5 Hz and the amplitude, defined as the displacement of the tip, reaches about 20° in total ( $\pm 10^\circ$ ). The experiment is repeated several times and steady-state oscillations in-phase and sometimes anti-phase are observed when using the same material (Fig. 1c,d and Supplementary Video 2). For the anti-phase synchronization, the frequency of the oscillation is 9.5 Hz  $\pm$  0.5 Hz. Similarly to the Huygens experiments on pendulum clocks<sup>13,14</sup>, the frequency of the in-phase oscillation is close to the frequency of a single oscillator of the same dimensions (about 8.5 Hz) and the frequency of anti-phase oscillation is slightly higher (9.5 Hz) due to the active participation of the coupling joint in the anti-phase synchronization. The phase diagrams of the oscillators represent an ellipse centred on the diagonal and the counter-diagonal, typical of in-phase and anti-phase harmonic oscillators, respectively (Fig. 1b). The difference in amplitudes between the two oscillators, as visible in Fig. 1c,d, may be related to differences in the light intensity reaching the hinge of each

oscillator. Indeed, it was reported previously that the light intensity affects the amplitude but not the frequency of the oscillation<sup>27</sup>. The obtention of in-phase or anti-phase oscillations comes from environmental changes, such as variation of temperature at the hinge controlled by the light position and the light intensity, or variation of the initial positions of the two synchronized oscillators. These results have been confirmed by the computer simulations presented below.

### Control experiments

Control experiments were performed to understand the origin of the coupling (Supplementary Video 3). When the light beam is focused exclusively on one strip, only the irradiated strip oscillates, and the other strip does not move. Likewise, when a strip consisting of the same material but polymerized in its isotropic state is joined to an oriented strip, upon irradiation the oriented strip oscillates while the strip without molecular orientation stays in the rest position and does not move. Moreover, when the common part of the LCN at the hinge is cut to obtain two independent strips, and the strips are clamped by two different tweezers and brought close together (about 2 mm), the oscillations are non-synchronized (neither in-phase nor anti-phase) indicating that the coupling is not derived from air dynamics. When the joint strips are clamped with a rigid pair of tweezers directly to the coupling element, resulting in a rigid joint giving a weak coupling, also no synchronization was observed. In addition to the presence of the coupling element, the influence of the width of the slit ( $w_g$ ) has been studied. The synchronization was observed with  $w_g$  as small as possible within the conditions of the experiments ( $w_g = 2$  mm). Having  $w_g$  smaller than 2 mm resulted in the two strips touching each other and disturbing the motion. Increasing  $w_g$  to 10 mm resulted in non-synchronized oscillations, showing that the coupling is dependent of  $w_g$ . These results indicate that the coupling strength decreases with the distance between the oscillators and confirm that the coupling occurs through the common LCN piece of film at the hinge. Overall, these control experiments stress an important prerequisite for synchronization; the two strips must be able to oscillate independently. Entrainment was not observed between one light-responsive strip capable of oscillating and one non light-responsive. It seems the coupling strength is not strong enough to trigger the oscillation of another strip.

### Temperature variation during the motion

Temperature is an important parameter in the mechanism of oscillation of these LCNs<sup>27</sup> and it was recorded during the motion. As reported for the single oscillator<sup>27</sup>, thermal oscillations were observed on the two strips. The in-phase mechanical oscillation gave in-phase thermal oscillation whereas the anti-phase mechanical oscillation gave anti-phase thermal oscillation (Extended Data Fig. 1). Possible thermal coupling was considered but the thermal conductivity of the LCN is poor (Extended Data Fig. 2) and the thermal oscillations are precisely localized on each strip. It was therefore concluded that the two hinge sections do not influence the temperatures of one another. One may note that the hinge is also irradiated and heated up in the steady state of synchronized oscillations (Extended Data Fig. 1c).

### Synchronized motion of asymmetric oscillators

The dynamics of the system were also studied with asymmetric oscillators of unequal lengths (Fig. 2a). We reported previously that the frequency of the oscillations depends on the length of the oscillators<sup>28</sup>. An oscillator 18 mm long oscillates at about 5.5 Hz  $\pm$  0.5 Hz (Fig. 2c, blue trace, and Supplementary Video 4), and shortening the film down to 12 mm gives an oscillation at about 10.1 Hz  $\pm$  0.5 Hz (Fig. 2c, orange trace, and Supplementary Video 5). When these two oscillators with lengths of 18 mm and 12 mm, respectively,

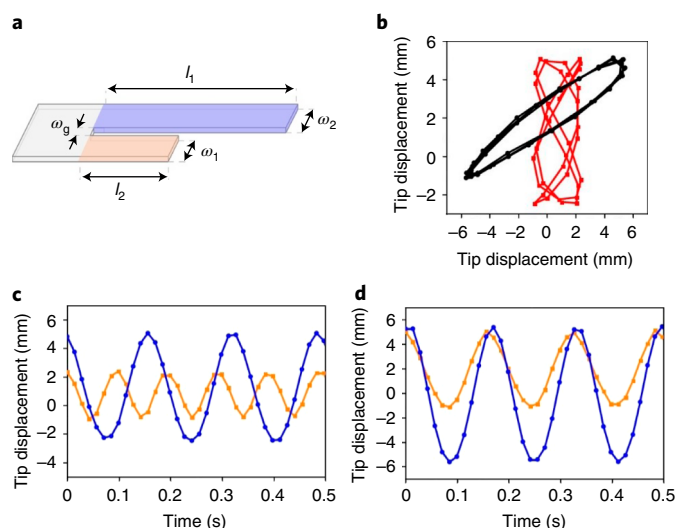


**Fig. 2 | Entrainment of asymmetric oscillators.** **a**, Schematic representation of the asymmetric films. The film geometry is 18 mm ( $l_1$ , in blue)  $\times$  12 mm ( $l_2$ , in orange)  $\times$  4 mm ( $w_1 = w_2$ )  $\times$  2 mm ( $w_2$ ). The sample thickness is 20  $\mu$ m. **b**, Phase diagrams of the uncoupled (red trace) and coupled (black trace) oscillators. **c**, Oscillation of the decoupled short and long oscillators. **d**, Oscillation of the coupled long and short oscillators. The displacement of the short oscillator is represented with the orange traces and that of the long oscillator with the blue traces.

are coupled, they oscillate at the same frequency of  $6.2 \text{ Hz} \pm 0.5 \text{ Hz}$  (Fig. 2d and Supplementary Video 6). The phase diagrams in Fig. 2b capture the difference between the coupled and non-coupled asymmetric oscillators, with the coupled oscillators giving an ellipse centred on the diagonal. These results demonstrate that one oscillating strip can entrain<sup>31</sup> a shorter strip to oscillate slower than its natural frequency. The long oscillator moves at about the same frequency when coupled or uncoupled. This experiment also shows the robustness of the coupling mechanism, as it is resistant to variations in the oscillators' length. Next to variation of the length, the frequency of the oscillations was found to be independent of the width of the oscillators, in correspondence to the theory around the natural frequency<sup>27</sup>, making an exact adjustment of  $w_1 = w_2$  unnecessary. Moreover, strips thicker than 20  $\mu$ m and wider than 5 mm do not oscillate because of their increased stiffness, which considerably limits the possibility to explore synchronization between asymmetric strips of unequal widths and thicknesses.

### Modelling of the synchronized motion

To gain insights into the mechanism of this synchronization and its origin, we carried out modelling of the coupled oscillators. The thin film is modelled as a standard spring-damper mechanical oscillator and the equation of motion is derived from the Euler–Lagrange method (Fig. 3a; Methods)<sup>32</sup>. The body of the film is represented by a rigid thin plate. The elements that contribute to the dynamic property in the model include an actuation torque and a viscoelastic torsional spring-damper element in the hinge. The spring-damper element is defined by a stiffness parameter ( $k(T) = \alpha \times E'(T)$ , with  $E'$  the storage modulus of the LCN film and  $\alpha$  the stiffness scaling parameter) and a damping parameter ( $d(T) = \beta \times E''(T)$ , with  $E''$  the loss modulus of the LCN film and  $\beta$  the damping scaling parameter). The stiffness and damping parameters depend on the temperature ( $T$ ), and their equations were derived from experimental mechanical tests where we took the temperatures as measured by the infrared camera as input (Extended Data Fig. 3). Eventual

photosoftening effects are ignored as thermal cycling takes place well above the glass transition temperature where the moduli are less temperature sensitive<sup>33</sup>. The actuation is modelled as the torque at the hinge and determined by the temperature dynamics of the LCN film (Extended Data Figs. 4 and 5). As is evident from the overlap between the experimental and calculated oscillations obtained (Extended Data Fig. 6), this model sufficiently describes the system with the stiffness and damping parameters reported in Supplementary Table 1. To proceed with the coupled oscillators, a coupling element was incorporated in the form of a torsional spring-damper element located in the hinge between the two oscillators. This coupling element is also characterized by a stiffness parameter  $k_{\text{coupling}}$  and a damping parameter  $d_{\text{coupling}}$  (Methods). The initial positions for the simulations, that is, angles, angular velocities and temperatures are set to be either randomized or fixed between the boundaries of the oscillation space.

The results of the simulations demonstrate good qualitative agreement with the experiments. The two oscillators synchronize their motion into two steady eigenmodes of the system: in-phase and anti-phase oscillations (Fig. 3b,c). The in-phase synchronization is more easily achieved than the anti-phase oscillation, indicating a difference in robustness and/or the corresponding basins of attraction between the two steady modes. The anti-phase simulated oscillation observed experimentally is also obtained in the simulated model although less perfectly. We investigated the influence of three parameters on the states of synchrony: the starting positions of the oscillators, the coupling stiffness parameter and the coupling damping parameter. A phase diagram was obtained by varying the coupling stiffness and damping parameters for fixed in-phase and anti-phase starting positions of  $\theta_1^0 = \theta_2^0$  and  $\theta_1^0 = -\theta_2^0$ , respectively (Fig. 3d). We show that, depending on the strength of the coupling, the solutions are stable or unstable in the sense of Lyapunov, that is, the solutions initiated close enough to each other remain close enough forever (stable states) or diverge (unstable states). For strong coupling, the model gives stable states with the solutions always being in-phase oscillation. These stable states are tolerant to changes in initial positions (Fig. 3e). Indeed, by varying the initial positions of the two oscillators, the model shows that the final state in-phase synchronization does not change. Even when the two oscillators start in anti-phase positions, they converge into in-phase synchrony, showing that the convergence of the in-phase mode is independent of the initial positions. However, for weak coupling, the model gives unstable states that switch between steady in-phase or anti-phase synchrony, depending on the initial positions for the same coupling parameters (Extended Data Figs 7 and 8). In other words, for weak coupling, small perturbations of the initial positions of the oscillators bring the system into different steady-state solutions (in-phase and anti-phase). Experimentally, this instability is visible when synchrony in-phase and anti-phase are observed with the same material. It did not escape our attention that occasionally even more complex coupling modes can be observed (Extended Data Fig. 9 and Supplementary Video 7). Altogether, these results show that slight variations of coupling stiffness, coupling damping and starting positions can change the mode of synchrony between in-phase and anti-phase motion, and confirm the experimental observations. Such variation of stiffness, damping and starting positions in the system could emerge from environmental changes such as temperature fluctuations at the hinge originating from changes in light position and light intensity, and dynamics effects.

### Outlook

In conclusion, we discovered that two joint LCN oscillators, driven by light, communicate together and synchronize their oscillations, as Huygens observed with pendulum clocks<sup>12,13</sup>. The synchronization originates from a mechanical coupling in the joint of

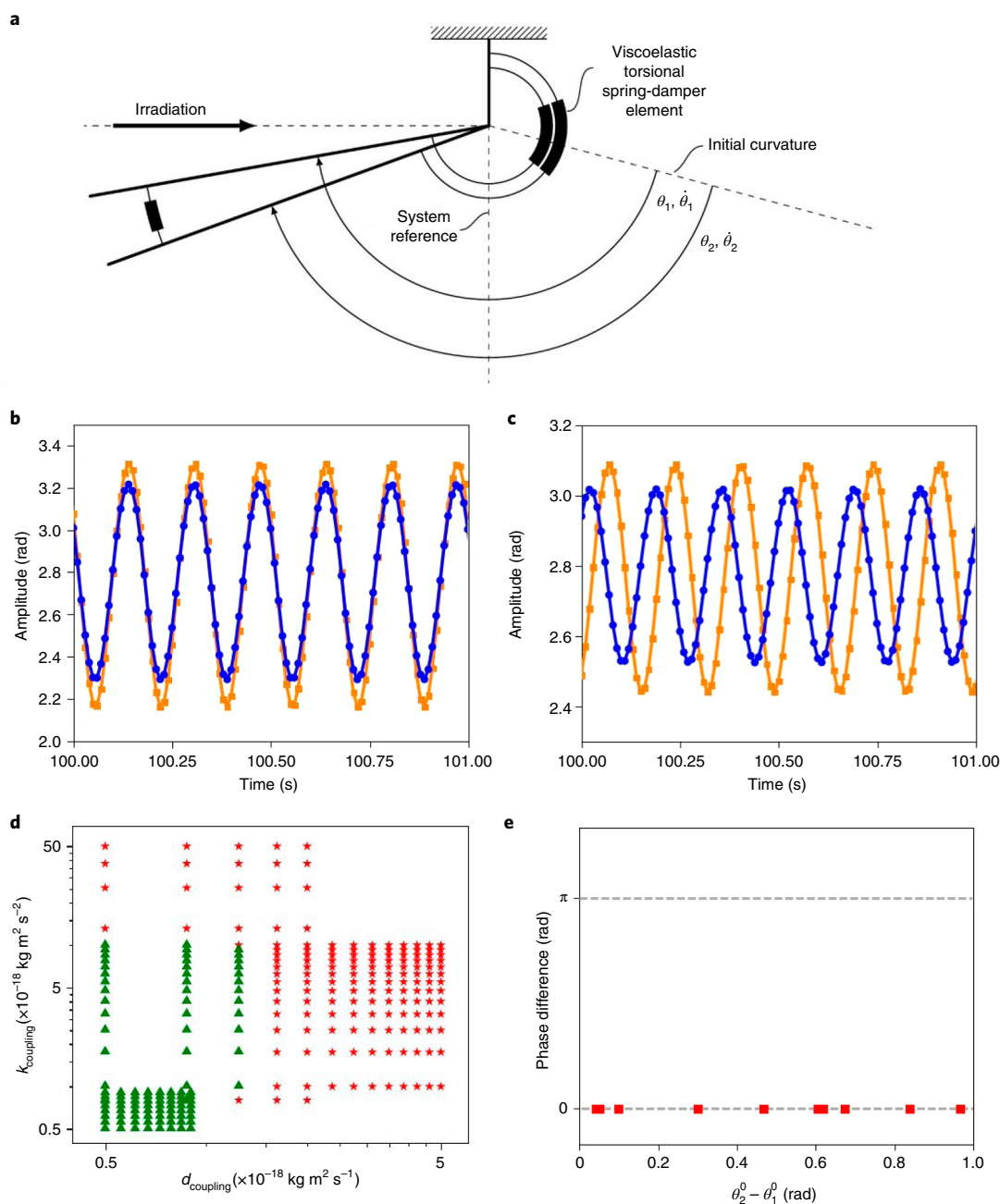


**Fig. 3 | Modelling of the coupled oscillators.** **a**, A schematic representation of the forced, damped coupled oscillator model. **b**, Simulations showing in-phase oscillations. **c**, Simulations showing anti-phase oscillations. The simulations are given in the steady states. **d**, The phase diagram with the coupling stiffness parameter  $k_{\text{coupling}}$  versus the coupling damping parameter  $d_{\text{coupling}}$ . The data points giving in-phase oscillation are represented by red stars and the ones giving an unstable state by green triangles. **e**, The phase difference between the coupled oscillations as a function of the difference in the initial positions of the two oscillators.

the oscillators and is sensitive to changes in the stiffness and the damping of the joint. Therefore, such a system could be used as sensors of the mechanical properties of materials. Synchronization and collective motion are a fascinating expression of self-organization that nature uses to sustain life. Mimicking such properties in life-like materials is a challenge undertaken at all length scales, from the nanoscopic<sup>34–37</sup> to the macroscopic. This work contributes to these on-going efforts to translate molecular events into macroscopic effects and proposes a general approach to create collective motion in polymeric materials. It is foreseen that these

results can be of great value in the fascinating developments in soft robotics.

#### Online content

Any methods, additional references, Nature Research reporting summaries, source data, extended data, supplementary information, acknowledgements, peer review information; details of author contributions and competing interests; and statements of data and code availability are available at <https://doi.org/10.1038/s41563-021-00931-6>.

Received: 6 March 2020; Accepted: 15 January 2021;  
Published online: 18 February 2021

## References

- Whitesides, G. M. Soft robotics. *Angew. Chem. Int. Ed.* **57**, 4258–4273 (2018).
- Zhang, X. et al. The pathway to intelligence: using stimuli-responsive materials as building blocks for constructing smart and functional systems. *Adv. Mater.* **31**, e1804540 (2019).
- Yu, Y. & Ikeda, T. Soft actuators based on liquid-crystalline elastomers. *Angew. Chem. Int. Ed.* **45**, 5416–5418 (2006).
- Hines, L., Petersen, K., Lum, G. Z. & Sitti, M. Soft actuators for small-scale robotics. *Adv. Mater.* **29**, 1603483 (2017).
- Martella, D., Nocentini, S., Parmeggiani, C. & Wiersma, D. S. Self-regulating capabilities in photonic robotics. *Adv. Mater. Technol.* **4**, 1800571 (2019).
- Zeng, H., Wasylczyk, P., Wiersma, D. S. & Priimagi, A. Light robots: bridging the gap between microrobotics and photomechanics in soft materials. *Adv. Mater.* **30**, 1703554 (2018).
- Hu, Y., Li, Z., Lan, T. & Chen, W. Photoactuators for direct optical-to-mechanical energy conversion: from nanocomponent assembly to macroscopic deformation. *Adv. Mater.* **28**, 10548–10556 (2016).
- Pikovsky, A., Rosenblum, M. & Kurths, J. *Synchronization: A Universal Concept in Nonlinear Sciences* (Cambridge Univ. Press, 2001).
- Vicsek, T. & Zafeiris, A. Collective motion. *Phys. Rep.* **517**, 71–140 (2012).
- Boccaletti, S. (ed.) *The Synchronized Dynamics of Complex Systems (Monograph Series on Nonlinear Science and Complexity)* Vol. 6 (Elsevier, 2008).
- O’Keeffe, K. P., Hong, H. & Strogatz, S. H. Oscillators that sync and swarm. *Nat. Commun.* **8**, 1504 (2017).
- Huygens, C. *Oeuvres complètes de Christiaan Huygens. L’horloge à pendule de 1651 à 1666. Travaux divers de physique, de mécanique et de technique de 1650 à 1666. Traité des couronnes et des parhélies (1662 ou 1663)* (La Société hollandaise des sciences, 1888).
- Bennett, M., Schatz, M. F., Rockwood, H. & Wiesenfeld, K. Huygens’s clocks. *Proc. R. Soc. A Math. Phys. Eng. Sci.* **458**, 563–579 (2002).
- Peña Ramirez, J., Olvera, L. A., Nijmeijer, H. & Alvarez, J. The sympathy of two pendulum clocks: Beyond Huygens’ observations. *Sci. Rep.* **6**, 23580 (2016).
- Ikeguchi, T. & Shimada, Y. Analysis of synchronization of mechanical metronomes. In *Proc. 5th International Conference on Applications in Nonlinear Dynamics* (eds In, V. et al.) 141–152 (Springer, 2019).
- Rubenstein, M. et al. Programmable self-assembly in a thousand-robot swarm. *Science* **345**, 795–799 (2014).
- Li, S. et al. Particle robotics based on statistical mechanics of loosely coupled components. *Nature* **567**, 361–365 (2019).
- Justus, K. B. et al. A biosensing soft robot: autonomous parsing of chemical signals through integrated organic and inorganic interfaces. *Sci. Robot.* **4**, eaax0765 (2019).
- Ciui, B. et al. Chemical sensing at the robot fingertips: toward automated taste discrimination in food samples. *ACS Sens.* **3**, 2375–2384 (2018).
- Korevaar, P. A. et al. Non-equilibrium signal integration in hydrogels. *Nat. Commun.* **11**, 386 (2020).
- Martella, D. et al. Photonic microhand with autonomous action. *Adv. Mater.* **29**, 1704047 (2017).
- Wani, O. et al. A light-driven artificial flytrap. *Nat. Commun.* **8**, 15546 (2017).
- Byun, J. et al. Electronic skins for soft, compact, reversible assembly of wirelessly activated fully soft robots. *Sci. Robot.* **3**, eaas9020 (2018).
- Yang, J. C. et al. Electronic skin: recent progress and future prospects for skin-attachable devices for health monitoring, robotics, and prosthetics. *Adv. Mater.* **31**, 1904765 (2019).
- Zhang, M. et al. Synchronization of micromechanical oscillators using light. *Phys. Rev. Lett.* **109**, 233906 (2012).
- White, T. J. & Broer, D. J. Programmable and adaptive mechanics with liquid crystal polymer networks and elastomers. *Nat. Mater.* **14**, 1087–1098 (2015).
- Gelebart, A. H., Vantomme, G., Meijer, E. W. & Broer, D. J. Mastering the photothermal effect in liquid crystal networks: a general approach for self-sustained mechanical oscillators. *Adv. Mater.* **29**, 1606712 (2017).
- Vantomme, G., Gelebart, A. H., Broer, D. J. & Meijer, E. W. Self-sustained actuation from heat dissipation in liquid crystal polymer networks. *J. Polym. Sci. Part A Polym. Chem.* **56**, 1331–1336 (2018).
- White, T. J. et al. A high frequency photodriven polymer oscillator. *Soft Matter* **4**, 1796–1798 (2008).
- Vantomme, G., Gelebart, A. H., Broer, D. J. & Meijer, E. W. A four-blade light-driven plastic mill based on hydrazone liquid-crystal networks. *Tetrahedron* **73**, 4963–4967 (2017).
- Cafferty, B. J. et al. Robustness, entrainment, and hybridization in dissipative molecular networks, and the origin of life. *J. Am. Chem. Soc.* **141**, 8289–8295 (2019).
- Peña Ramirez, J., Fey, R. H. B., Aihara, K. & Nijmeijer, H. An improved model for the classical Huygens’ experiment on synchronization of pendulum clocks. *J. Sound Vib.* **333**, 7248–7266 (2014).
- Shimamura, A. et al. Simultaneous analysis of optical and mechanical properties of cross-linked azobenzene-containing liquid-crystalline polymer films. *ACS Appl. Mater. Interfaces* **3**, 4190–4196 (2011).
- Merindol, R. & Walther, A. Materials learning from life: Concepts for active, adaptive and autonomous molecular systems. *Chem. Soc. Rev.* **46**, 5588–5619 (2017).
- Dattler, D. et al. Design of collective motions from synthetic molecular switches, rotors, and motors. *Chem. Rev.* **120**, 310–433 (2020).
- Leira-Iglesias, J., Tassoni, A., Adachi, T., Stich, M. & Hermans, T. M. Oscillations, travelling fronts and patterns in a supramolecular system. *Nat. Nanotechnol.* **13**, 1021–1027 (2018).
- Boekhoven, J., Hendriksen, W. E., Koper, G. J. M., Eelkema, R. & Van Esch, J. H. Transient assembly of active materials fueled by a chemical reaction. *Science* **349**, 1075–1079 (2015).

**Publisher’s note** Springer Nature remains neutral with regard to jurisdictional claims in published maps and institutional affiliations.

© The Author(s), under exclusive licence to Springer Nature Limited 2021

## Methods

**Materials and fabrication of the films.** We prepared LCNs by the photopolymerization of a mixture of commercially available mesogens RM82 (60 wt%) and RM23 (37.5 wt%), the photo-active component (hydroxyphenyl) benzotriazole (Tinuvin 328, 2.5 wt%, Extended Data Fig. 10) and a photo-initiator (Irgacure 819, <1 wt%). The chemicals were obtained from Merck. The method to prepare thin films has been precisely reported elsewhere<sup>38</sup>. Before polymerization, the mesogens are aligned in splay fashion by the use of polyimide alignment layers in custom-made cells. The splay alignment consists of a planar alignment on one side of the film, and a homeotropic alignment on the other side, with a gradual change in the molecular orientation over the 20  $\mu\text{m}$  thickness of the film. The glass transition temperature of the film is about 45  $^{\circ}\text{C}$ . The moduli are reported in Extended Data Fig. 3. For the control experiment where a strip consisting of the same material but polymerized in its isotropic state is joined to an oriented strip, photopolymerization by a mask exposure is performed. First, the mixture is photopolymerized through a mask at 70  $^{\circ}\text{C}$  (LC phase) for 5 s. Then the mask is removed, the temperature is increased to 110  $^{\circ}\text{C}$  (isotropic phase) and the photopolymerization is completed on the entire substrate.

**Photo-actuation.** The films were peeled off from the glass substrate of the cell and cut using a razor blade into two long strips connected by a joint of the same material (Fig. 1a), with the alignment director of the mesogens parallel to the long edge. The two parallel strips were clamped by the hinge, with the side of planar molecular alignment facing the lamp and simultaneously irradiated with an LED mounted with a collimator (Thorlabs) emitting 365 nm (0.5  $\text{W cm}^{-2}$ ). Upon irradiation, the films bend toward the light and, after a few seconds, the two films show a steady self-oscillation.

**Characterization of the films and the motion.** The temperature of the films was reported with a high-speed thermal camera Gobi from Xenics. The videos of the oscillations were recorded by a PCO 5.5 sCMOS camera and the recordings were further treated with software of image analysis.

The moduli of the films were determined using a Q800 machine by TA Instruments.

**Modelling of the motion derived from the Euler–Lagrange method.** First, we derive the equations of motion for the single LCN oscillator. This model will be extended later on towards the case of double oscillators. Let  $\theta_{\text{IC}}$  stand for the angle of the free oscillator which corresponds to the steady-state equilibrium of the irradiated film. Let  $T$  stand for the temperature of the hinge. The kinetic energy of the film is defined as

$$K(\dot{\theta}) = \frac{1}{2}J\dot{\theta}^2, \quad (1)$$

where  $J$  is the corresponding inertia moment. The potential energy is defined then as

$$V(\theta) = \frac{1}{2}k\theta^2 + \frac{1}{2}(gIm(\cos(\theta_{\text{IC}} - \theta) - 1)), \quad (2)$$

where  $g$  is the acceleration due to gravity,  $m$  is the mass of the film,  $l$  is the length of the film and  $k$  is the stiffness of the torsion spring.

Subsequently, the Lagrangian of the system is constructed as

$$L(\theta, \dot{\theta}) = K(\dot{\theta}) - V(\theta) \quad (3)$$

and the Euler–Lagrange equations

$$\frac{d}{dt}\left(\frac{\partial L}{\partial \dot{\theta}}\right) - \left(\frac{\partial L}{\partial \theta}\right) = Q^{\text{nc}} \quad (4)$$

have the following form

$$\ddot{\theta} = \frac{1}{J}\left(Q^{\text{nc}} - k\theta - \frac{1}{2}mgl \sin(\theta - \theta_{\text{IC}})\right). \quad (5)$$

Here the non-conservative terms are given by

$$Q^{\text{nc}} = u - d\dot{\theta}, \quad (6)$$

with  $d$  being the damping factor and  $u$  the temperature dependent torque at the hinge.

In a similar fashion one can derive a dynamical model for two coupled LCN films. We assume that the films are coupled via a torsion spring and damper, which is a mechanically more advanced flexible coupling previously reported<sup>32</sup>. In other words, there is an extra potential energy associated with the angular difference of two oscillators:

$$V_{\text{coupling}} = \frac{1}{2}k_{\text{coupling}}(\theta_1 - \theta_2)^2. \quad (7)$$

With this assumption the model of coupled identical oscillators is given by the following two second-order differential equations:

$$\ddot{\theta}_1 = \frac{1}{J}(u_1 - d\dot{\theta}_1 - k\theta_1 - d_{\text{coupling}}(\dot{\theta}_1 - \dot{\theta}_2) - k_{\text{coupling}}(\theta_1 - \theta_2) - \frac{1}{2}mgl \sin(\theta_1 - \theta_{\text{IC}})) \quad (8)$$

$$\ddot{\theta}_2 = \frac{1}{J}(u_2 - d\dot{\theta}_2 - k\theta_2 - d_{\text{coupling}}(\dot{\theta}_2 - \dot{\theta}_1) - k_{\text{coupling}}(\theta_2 - \theta_1) - \frac{1}{2}mgl \sin(\theta_2 - \theta_{\text{IC}})) \quad (9)$$

The inertia moment of the oscillators  $J$  is calculated under the assumption that each film is a rigid lamina:

$$J = \frac{1}{3}ml^2, \quad (10)$$

$$m = \rho hwl \quad (11)$$

where  $\rho$  is the film density and  $h, w$  are the height and the width of the film, respectively (Supplementary Table 1).

The stiffness and damping of the spring-damper elements of the model are designed to be proportional to the storage and loss moduli of the LCN, respectively.

The stiffness and damping coefficients  $k$  and  $d$  of the spring-damper elements are defined as:

$$k(T) = \alpha E'(T) \quad (12)$$

and

$$d(T) = \beta E''(T) \quad (13)$$

respectively (Extended Data Fig. 3), where  $\alpha$  is the stiffness scaling parameter and  $\beta$  is the damping scaling parameter (Supplementary Table 1).

The torque  $u_i$ ,  $i = 1, 2$ , generated by the hinge heating is modelled as a linear function of the hinge temperature:

$$u_i(T_i) = v\left(\frac{T_i - T_{\text{amb}}}{T_{\text{max}}}\right), \quad i = 1, 2 \quad (14)$$

where  $v$  is the scaling parameter, and  $T_{\text{amb}}$  and  $T_{\text{max}}$  are the ambient and maximal temperatures, respectively (Supplementary Table 1).

The hinge temperature for each oscillator is modelled as the following first-order differential equation:

$$\dot{T}_i(\theta_i) = \frac{\Delta(T_i)}{2} \tanh(\mu(\theta_i - \theta_{\text{IC}} - \Phi)) + \lambda(T_i), \quad i = 1, 2 \quad (15)$$

where the functions  $\lambda(T)$  and  $\Delta(T)$  are defined as

$$\lambda(T) = \frac{1}{2}\left(\frac{T_{\text{max}} - T}{\tau_a} - \frac{T_{\text{amb}} - T}{\tau_d}\right), \quad (16)$$

$$\Delta(T) = \frac{T_{\text{amb}} - T}{\tau_d} - \frac{T_{\text{max}} - T}{\tau_a} \quad (17)$$

and the tuning parameters  $\tau_a, \tau_d$  are determined experimentally as  $\tau_a = 0.75$  s,  $\tau_d = 0.64$  s (Extended Data Fig. 5).

During the simulation, the values of the oscillator's geometrical properties, including length, width and thickness, are slightly randomized by  $\pm 1\%$  of its default. The randomization eliminates identity and causes the system to rely on synchronization induced by its mechanical coupling.

## Data availability

The data that support the findings of this study are available within the article and its Supplementary Information files, and from the corresponding authors upon reasonable request.

## References

38. Vantomme, G., Gelebart, A. H., Broer, D. J. & Meijer, E. W. Preparation of liquid crystal networks for macroscopic oscillatory motion induced by light. *J. Vis. Exp.* **127**, e56266 (2017).

## Acknowledgements

This work was financially supported by The Netherlands Organization for Scientific Research (NWO-TOP PUNT grant no. 10018944 and NWO-VENI grant no. 722.017.003), Dutch Ministry of Education, Culture and Science (Gravity Programme grant no. 024.001.035) and the European Research Council (Vibrate ERC grant no. 669991).

**Author contributions**

G.V., E.W.M. and D.J.B. conceived and planned the project. G.V. and A.H.G. performed the experiments. L.C.M.E. performed the simulations. D.J.B., H.N., A.Y.P. and E.W.M. supervised the effort. G.V. wrote the manuscript. All authors discussed the results and commented on the manuscript.

**Competing interests**

The authors declare no competing interests.

**Additional information**

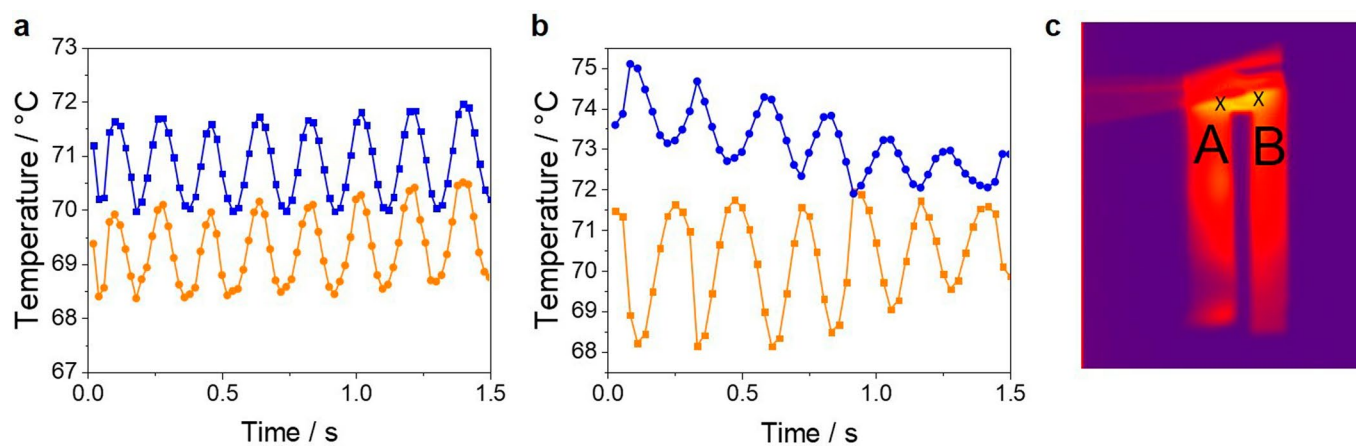
**Extended data** is available for this paper at <https://doi.org/10.1038/s41563-021-00931-6>.

**Supplementary information** The online version contains supplementary material available at <https://doi.org/10.1038/s41563-021-00931-6>.

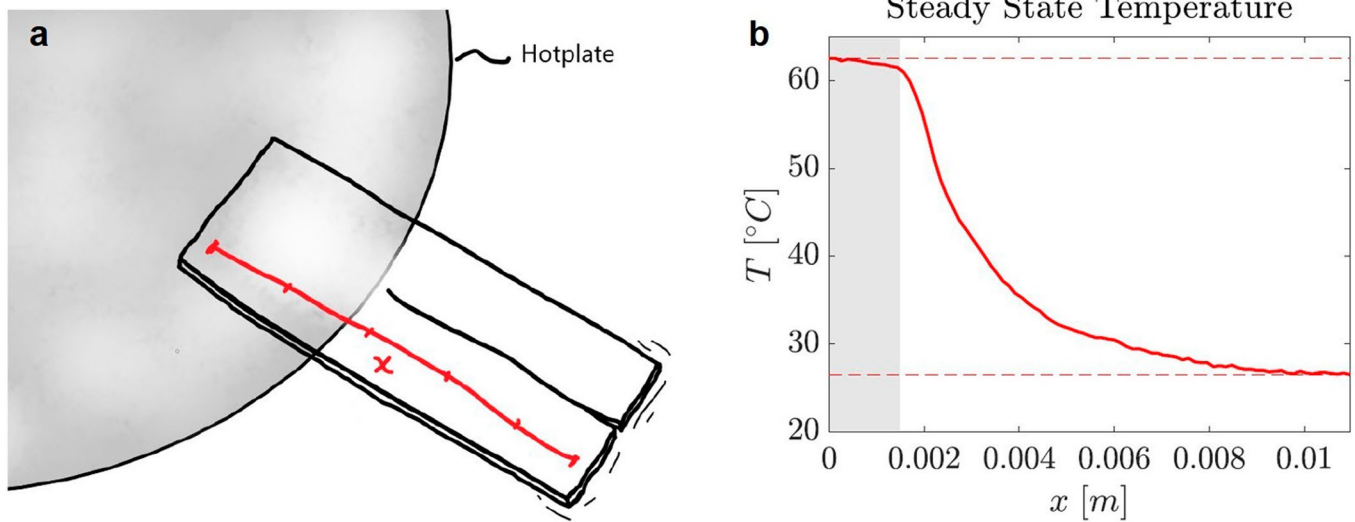
**Correspondence and requests for materials** should be addressed to G.V. or D.J.B.

**Reprints and permissions information** is available at [www.nature.com/reprints](http://www.nature.com/reprints).

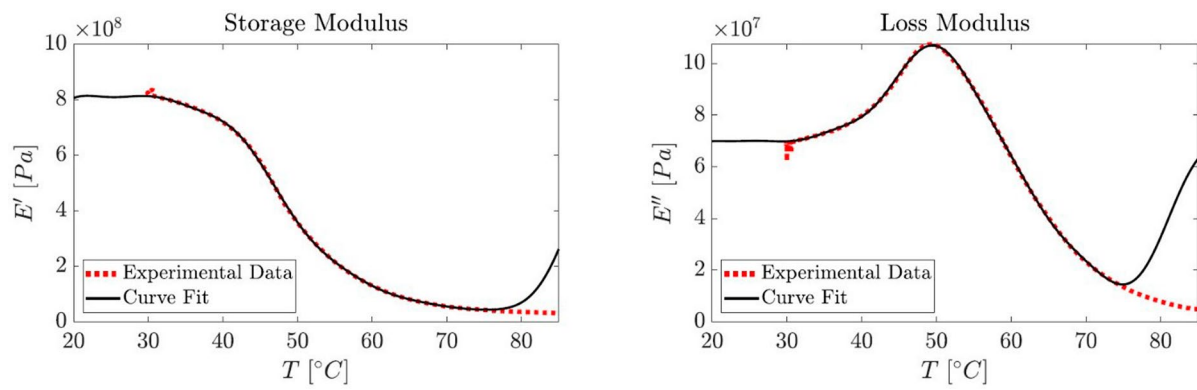




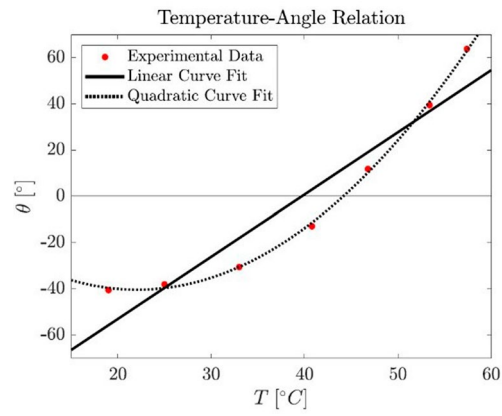
**Extended Data Fig. 1 | Thermal oscillation.** **a,b**, Temperature of the coupled LCN films during in-phase oscillation (**a**) and anti-phase oscillation (**b**). **c**, Picture of the thermogram with the two points A and B where the temperatures are measured. The temperature at point A is the blue trace and at point B is the orange trace. The films geometry is 20 mm × 4 mm × 20 μm and are connectively separated by 2 mm.



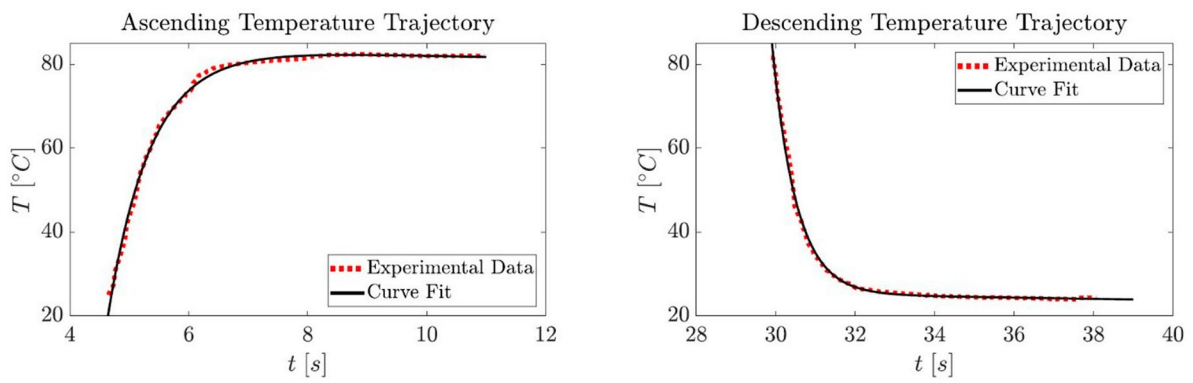
**Extended Data Fig. 2 | Thermal conductivity.** **a**, Scheme of the LCN film positioned on a hot plate at 63 °C. **b**, Temperature profile over the length of the film showing the poor thermal conductivity of the LCN.



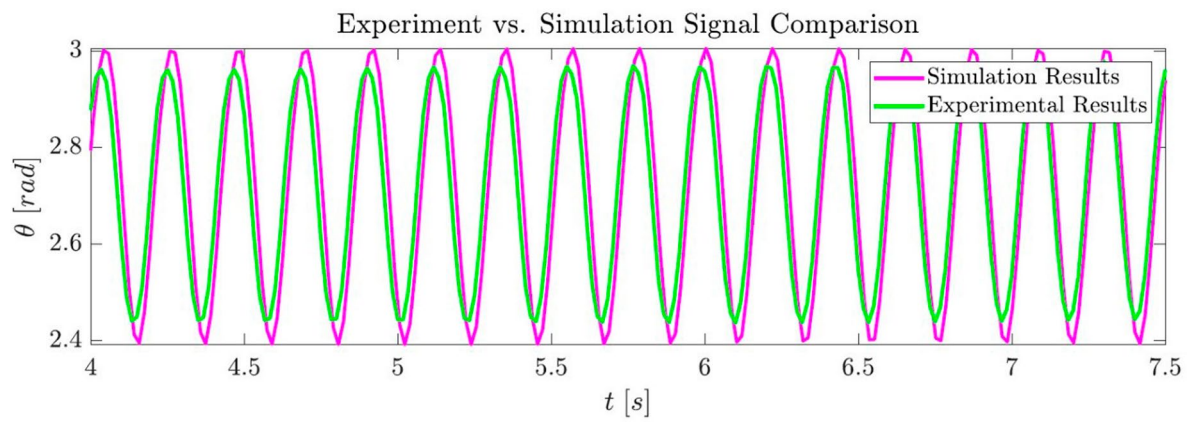
**Extended Data Fig. 3 | Modeling of the stiffness and damping parameters.** Tensile moduli of the LCN film as a function of temperature (red traces) and their modeled fits (black traces).



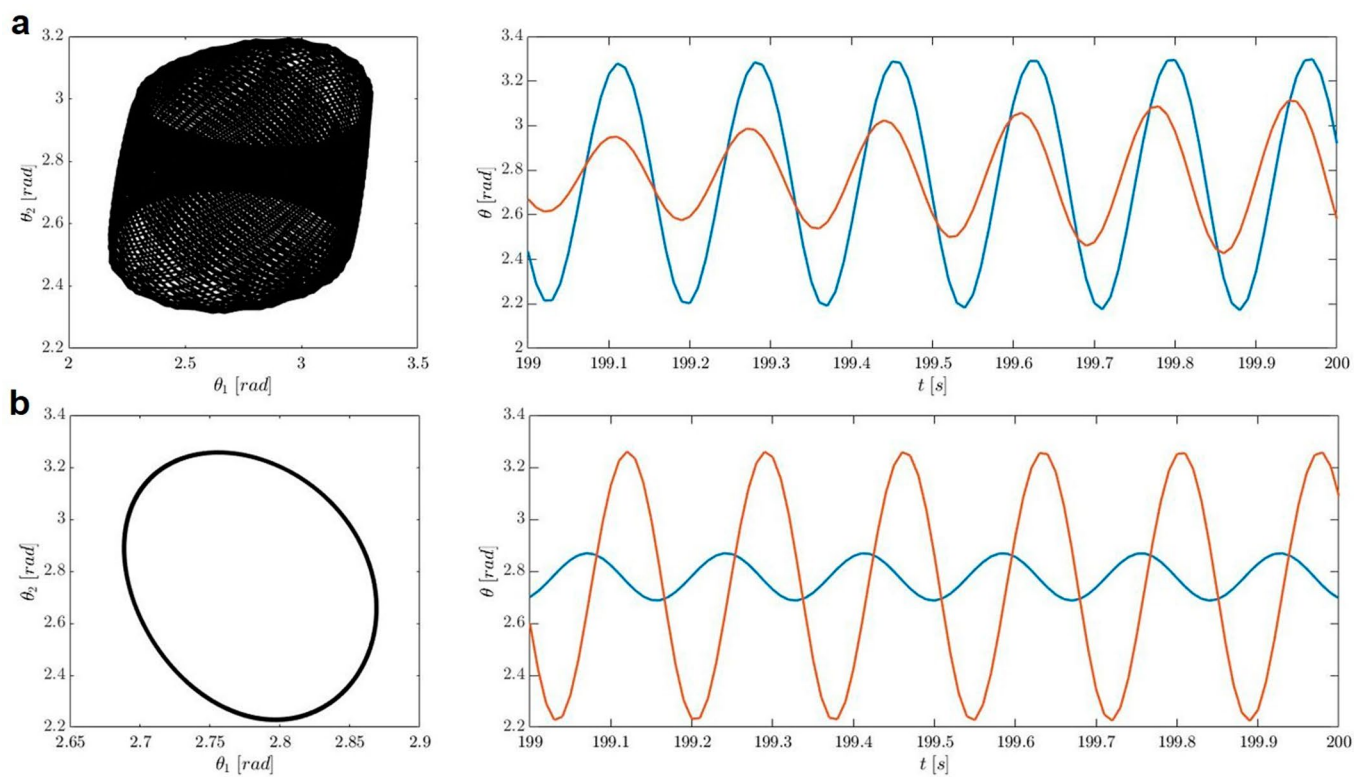
**Extended Data Fig. 4 | Modeling of the actuation torque with temperature.** Displacement of the film tip over temperature (dotted line) and the linear fit obtained (black trace).



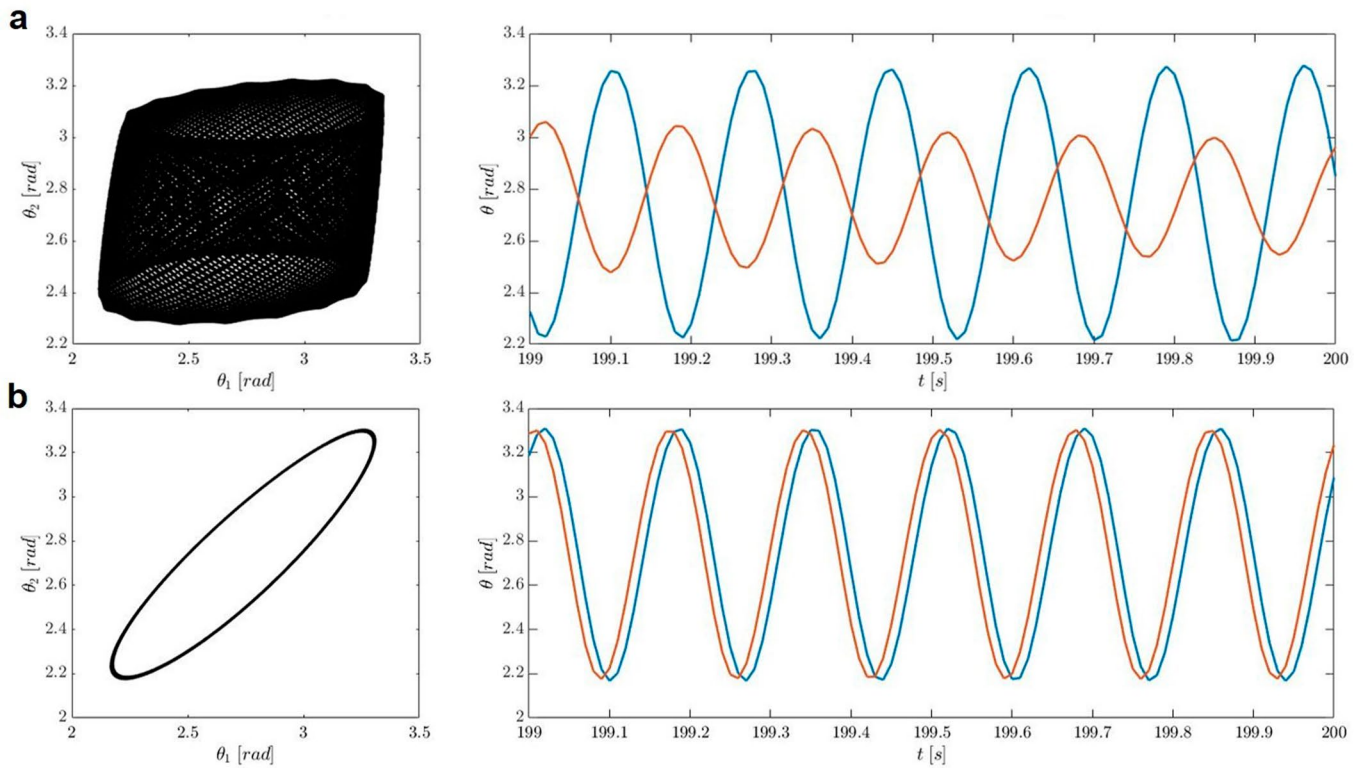
**Extended Data Fig. 5 | Modeling of the temperature dynamics.** Temperature of the LCN film upon switching the LED on (*left*) and off (*right*). The experimental data are the red traces and the calculated fits are the black traces.



**Extended Data Fig. 6 | Comparison of the experimental and calculated oscillations.** Experimental (green trace) and simulation (magenta trace) results of the oscillation over time.

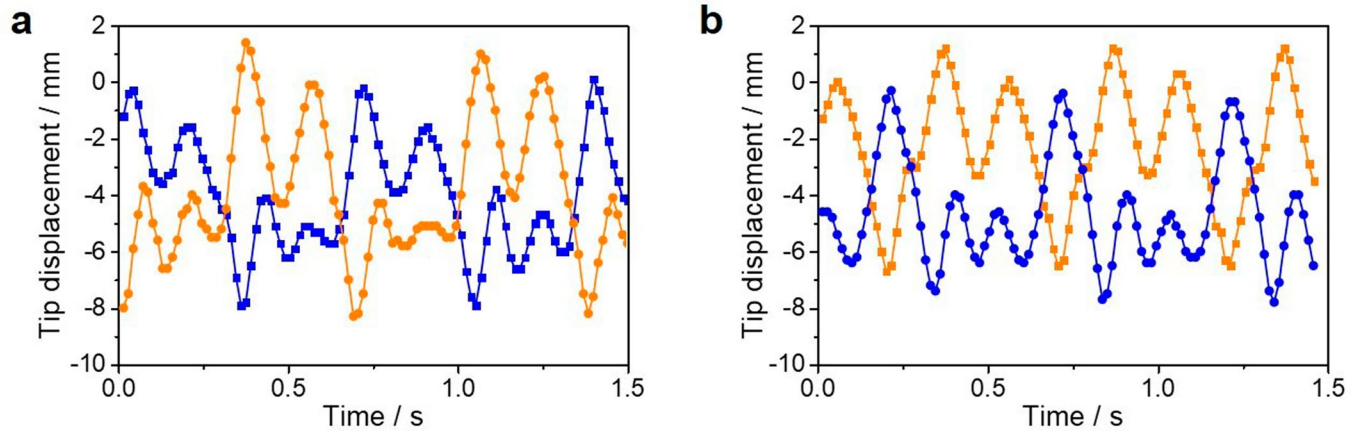


**Extended Data Fig. 7 | Modeling with a weak coupling showing changes in the final state depending on the starting conditions.** **a**, Example of non-periodic oscillations modeled with the coupling stiffness parameter  $k_{\text{coupling}} = 5 \times 10^{-19} \text{ kg.m}^2.\text{s}^{-2}$  and the coupling damping parameter  $d_{\text{coupling}} = 7.29 \times 10^{-19} \text{ kg.m}^2.\text{s}^{-1}$ , with the starting conditions  $\theta_1^0 = \theta_2^0 = 2.3 \text{ rad}$  showing instability and **b**, with the starting conditions  $\theta_1^0 = 2.6 \text{ rad}$  and  $\theta_2^0 = 3.3 \text{ rad}$  showing anti-phase oscillation.

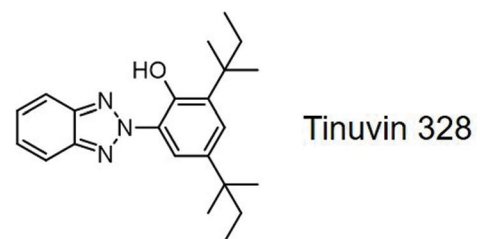
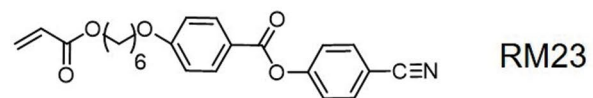
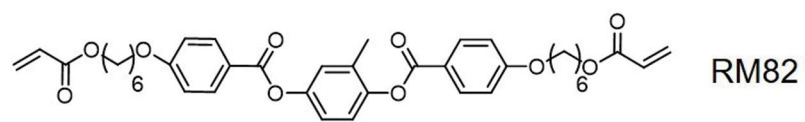


**Extended Data Fig. 8 | Modeling with a weak coupling showing changes in the final state depending on the starting conditions.** **a**, Example of non-periodic oscillations modeled with the coupling stiffness parameter  $k_{\text{coupling}} = 5 \times 10^{-19} \text{ kg.m}^2.\text{s}^{-2}$  and the coupling damping parameter  $d_{\text{coupling}} = 7.29 \times 10^{-19} \text{ kg.m}^2.\text{s}^{-1}$ , with the starting conditions  $\theta_1^0 = 3.1 \text{ rad}$  and  $\theta_2^0 = 2.3 \text{ rad}$  showing non-periodic oscillations and **b**, with the starting conditions  $\theta_1^0 = 2.9 \text{ rad}$  and  $\theta_2^0 = 2.6 \text{ rad}$  showing in-phase oscillation.





**Extended Data Fig. 9 | Complex synchronized motion of coupled LCN experimentally obtained.** **a**, Displacement of the tips of the two coupled oscillators over time in the z-direction. The displacement of one oscillator is represented with the orange trace and the other one with the blue trace. **b**, A different motion obtained stochastically after switching the LED on and off. The data reported in graphs **a** and **b** are plotted from two different sequences combined in Supplementary Video 7. The data plotted on graph **a** are from the first minute of Supplementary Video 7, and the data on the graph **b** are from the second sequence of Supplementary Video 7.



**Extended Data Fig. 10 | Molecular structures.** Structures of the reactive mesogens RM82 and RM23, and structure of the chromophore Tinuvin 328.